# Self-Texture in the Initial Stages of ZnO Film Growth

**M. H. Koch, A. J. Hartmann, and R. N. Lamb***

*Surface Science & Technology, School of Chemistry University of New South Wales, NSW 2052, Sydney, Australia*

**M. Neuber and M. Grunze**

*Angewandte Physikalische Chemie, Universität Heidelberg, Im Neuenheimer Feld 253, 69120 Heidelberg, Germany*

*Received: March 27, 1997*[⊗]

X-ray absorption spectroscopy has been used to investigate the self-texture of ZnO films grown on Si(100) (lattice-mismatched substrate) by single-source chemical vapor deposition (SS-CVD) using $Zn_4O(acetate)_6$ as precursor. For this system nonepitaxial growth of polycrystalline, *c*-axis oriented films can be controlled by addition of a water ambient during the deposition for a large variety of substrates. Angle dependent near edge X-ray absorption fine structure spectroscopy (NEXAFS) was used to study the orientation of the adsorbent molecules as a function of both water ambient used during the deposition and film thickness. The onset of self-structuring under optimum growth conditions (highest water pressure, $P_{H_2O} = 5 \times 10^{-4}$ mbar) is found to occur at film thicknesses on the order of 50 Å. The role of the water ambient during the film deposition is discussed using a kinetic model in which lattice stabilization due to filling of oxygen vacancies promotes the film crystallization. The model is used to explain the measured changes in the atomic environment of the oxygen atoms in the deposited ZnO films with variation in ambient water used. The interfacial restrictions in nonepitaxial CVD film growth are discussed. Our results indicate that in addition to structural restrictions due to lattice mismatch the chemical reactivity of the substrate material clearly must be considered.

## Introduction

ZnO films are widely used in various applications such as optical modulators, surface acoustic wave (SAW) devices, and coatings of solar cells. ZnO crystallizes in a hexagonal, wurtzite type structure with 6-mm symmetry.[1] The (0001) plane has the lowest surface free energy and is a singular surface of films in equilibrium state.[2] Therefore ZnO films grow with a strong (0001) preferred orientation, commonly referred to as *c*-axis-oriented films, on a variety of substrates. Such films consist of columnar grains of crystallites oriented with the *c*-axis perpendicular to the substrate.[1] When this film texture is obtained in the absence of epitaxial growth conditions (i.e. lattice match between substrate and film), it is referred to as self-texture. In the (0001) texture, optimum piezoelectric and electrooptic characteristics are obtained across the ZnO film in multilayer devices.[3,4] *c*-Axis-oriented films have been grown using different techniques such as rf-magnetron sputtering, CVD, or spray pyrolysis. The structure of the films is usually investigated using either reflection high-energy electron diffraction (RHEED) for thin, epitaxial grown ZnO films or X-ray diffraction (XRD) performed ex situ for thicker films $d \geq 50$ nm.[5,6]

We present for the first time an in situ X-ray absorption spectroscopy (XAS) and X-ray photoelectron spectroscopy (XPS) study of self-texture in ultrathin ZnO films grown on Si(100) using SS-CVD from a $Zn_4O(acetate)_6$ (basic zinc acetate, BZA) precursor. In CVD film growth from this precursor, a macroscopic film texture (determined using XRD) is only obtained upon addition of a water ambient during the deposition.[7] As a result, the deposition conditions required to promote self-textured growth of the ZnO films on the lattice-mismatched Si substrate can be controlled. The relatively low energy CVD technique is ideally suited to isolating the intrinsic interfacial restrictions of the substrate−film system as compared to higher energy sputter deposition techniques, where mechanical interactions between the impinging particles and the substrate must be considered. The combined use of XAS and XPS to study the initial stages of film growth could be established as a powerful experimental tool for a large variety of systems.

## Experimental Section

The measurements were performed at "Berliner Elektronen Speicherring-Gesellschaft für Synchrotronstrahlung", BESSY in Berlin, Germany. The monochromator used (HE-TEGM-2) provides synchrotron radiation in a photon energy range of $E_{Photon} = 100-900$ eV with a resolution of $E_{Photon}/\Delta E_{Photon} \approx 1000$. The carbon edge energy range was calibrated using the adventitious carbon absorption peak ($E_{Photon} = 285.0$ eV) in the monochromator transmission, $I_0(E_{Photon})$, whereas the oxygen edge energy range was calibrated using a CuO reference sample.[8] The NEXAFS data were obtained in partial yield electron detection mode, and surface-extended X-ray absorption fine structure (SEXAFS) data were collected in total yield mode. The data were processed and normalized as discussed by Hartmann et al.[9] The analysis chamber was a VG ESCASCOPE UHV chamber equipped with an Al Ka X-ray source, a hemispherical electron energy analyzer for XPS measurements, and a channeltron for detection of the electron yield in the X-ray absorption spectroscopy measurements.[10]

The ZnO films were deposited in an adjacent preparation chamber. The BZA precursor was sublimated in a modified Knudsen cell and the cell temperature adjusted to give a BZA partial pressure of approximately $5 \times 10^{-7}$ mbar. The water ambient was regulated through a leak valve connected to an evacuated dosing system. The films were deposited at 673 K

* Author for correspondence.
⊗ Abstract published in *Advance ACS Abstracts,* September 15, 1997.

S1089-5647(97)01088-2 CCC: $14.00 

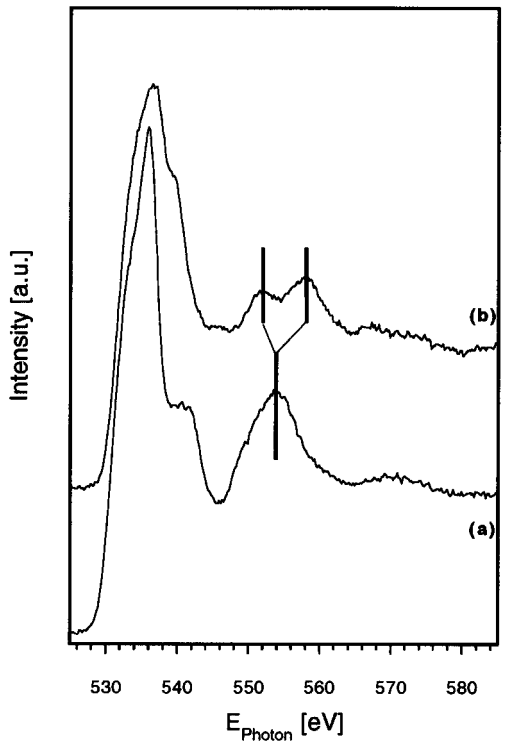


**Figure 1.** O 1s NEXAFS spectra for polycrystalline, *c*-axis-oriented ZnO film (thickness ~0.5 $\mu$m): (a) angle $\vartheta = 0°$ between the electric field vector of the synchrotron radiation and the surface plane; (b) $\vartheta = 60°$.

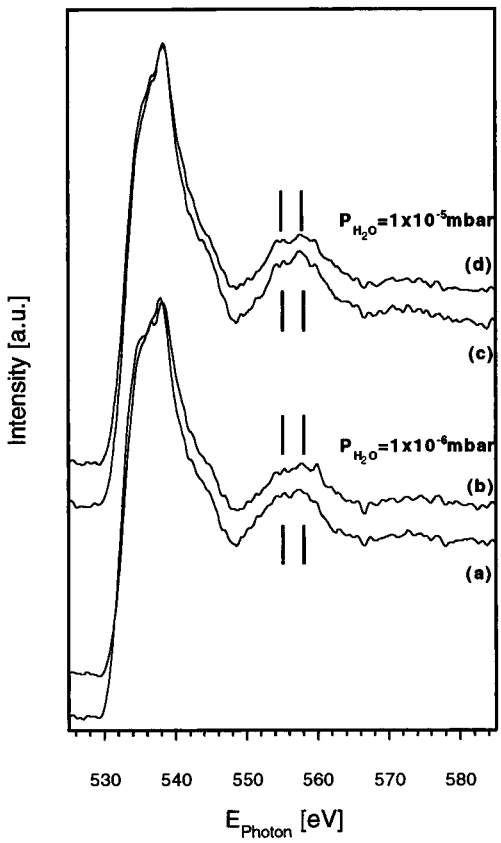


**Figure 2.** O 1s NEXAFS spectra for films deposited with medium water pressures at a surface temperature of 673 K for approximately 60 Å thick films: (a and c) angle $\vartheta = 0°$ between the electric field vector of the synchrotron radiation and the surface plane; (b and d) $\vartheta = 60°$.

substrate temperature, and the sample then transferred into the analysis chamber where it cooled to room temperature. Prior to each growth cycle, the Si(100) substrate was argon sputter cleaned and then annealed at 900 K. This procedure was found to create a substrate free of any major structural damages.[11] The cleanliness was controlled by XAS and XPS measurements. Film thicknesses reported were calculated using the attenuation of the Si substrate 2p photoelectron peak intensity. The accuracy of this method is on the order of 25%.[12] Previous studies[11,13] have shown that the continuous growth model for the present system is applicable for film thicknesses above 15 Å.

## Results and Discussion

**(1) Onset of Self-Texture.** Recently, the utilization of angle dependent NEXAFS measurements as a "fingerprint" of the symmetry type in films has been demonstrated.[14,15] In Figure 1 the O 1s NEXAFS measurements for a ~500 nm thick, polycrystalline and *c*-axis oriented ZnO reference film are shown for two different angles, $\vartheta$, between the electric field vector of the synchrotron radiation and the surface plane. For this orientation, the ZnO unit cells are arranged with the *c*-axis perpendicular to the substrate surface. The angle dependency of the NEXAFS spectra reflects the change of the direction of the transition dipole moment for the O 1s electron excitations into the partly empty $sp^3$ hybridized orbital at the oxygen sites of the ZnO matrix. The main features of the angle dependency are (i) splitting of the peak at ~554 eV in the spectrum for $\vartheta = 0°$ into two peaks at ~552 and ~558 eV in the spectrum for $\vartheta = 60°$ and (ii) a change in the high-energy shoulder structure of the main edge peak.

In Figures 2 and 3 O 1s NEXAFS spectra for ZnO films deposited with varying water pressures are shown for $\vartheta = 0°$ and $\vartheta = 60°$. For the spectra of the films deposited with $P_{H_2O} = 1 \times 10^{-6}$ mbar and $P_{H_2O} = 1 \times 10^{-5}$ mbar (Figure 2), no angle dependency of the spectra was found (film thicknesses were 80 and 65 Å, respectively). The features of the spectra in Figure 2 indicate that no preferred orientation of the $sp^3$ hybridized orbital at the oxygen sites exists in the deposited films. For a film with random orientation of the hybrid orbital the NEXAFS signal will be angle independent and the resulting spectrum should be similar to an average of the spectra obtained from the reference film at the two extreme angles (Figure 1). This would explain the obtained broadening of the main edge peak and the small, angle independent splitting (~3.5 eV) of the second peak in the spectra in Figure 2.

When the deposition is performed in a water ambient of $5 \times 10^{-4}$mbar (Figure 3), a small angle dependency of the NEXAFS signal similar to that for the ZnO reference film is obtained at a film thickness of 50 Å. These deposition conditions are comparable to those previously reported for growth of polycrystalline, *c*-axis-oriented ZnO films[7] (crystalline structure of 0.5−0.8 $\mu$m films confirmed by XRD). Our results show that under these growth conditions self-texture occurs at a film thickness on the order of 50 Å. The result that no preferred texture is obtained in the 30 Å thickness film deposited under the same conditions (Figure 3) could be related to the fact that during the initial stages of film growth some oxidation of the silicon substrate occurs (see XPS spectra in Figure 4). This results in a mixed interfacial region of this thickness range in the initial growth stages. We have reported in an earlier paper[11] that such an oxidation is also obtained when the deposition is performed in the absence of a water ambient. This was related to the formation of chemical bonds between oxygen-containing decomposition fragments and the "reactive" Si substrate. It was subsequently suggested that at 673 K substrate temperature the presence of oxygen-containing species at the surface might cause

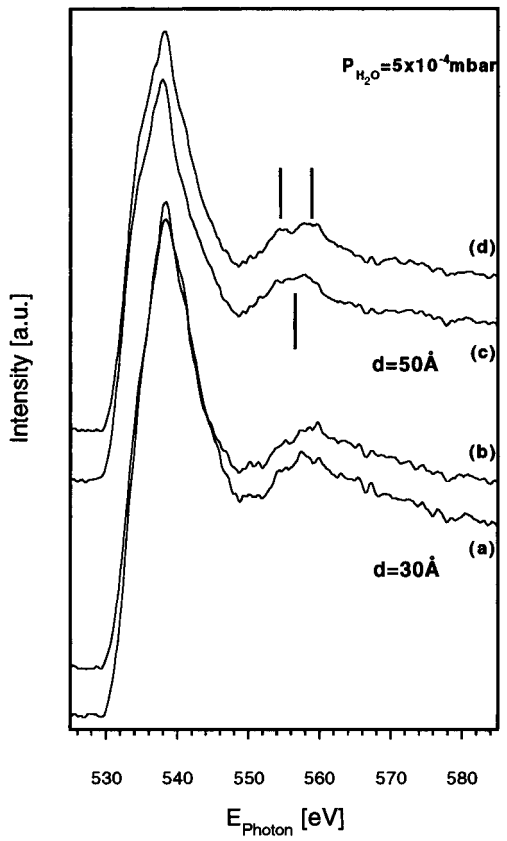


**Figure 3.** O 1s NEXAFS for deposition with a water ambient of $5 \times 10^{-4}$ mbar as a function film thickness, *d*, deposited at a surface temperature of 673 K: (a and c) angle $\vartheta = 0°$ between the electric field vector of the synchrotron radiation and the surface plane; (b and d) $\vartheta = 60°$.

some diffusion of Si (high oxidation potential) into the film, forming a mixed interfacial region comprising both ZnO and oxidized silicon species. This would inhibit growth of "pure", textured ZnO films from the immediate substrate−film interface.

To gain further information about the molecular structure in the deposited films, we also analyzed the SEXAFS region of the O 1s absorption edge. In the region above approximately 50 eV from the edge, the absorption coefficient, $\mu$, oscillates due to the interference of the emitted photoelectron wave with neighboring atoms. The change of the absorption coefficient compared to the value for the free atom, $\mu_0$, can be expressed as a function of the propagation constant of the emitted photoelectron wave, *k*, chi(*k*) = $[\mu(k) - \mu_0(k)]/\mu_0$. The radial distribution function (RDF) of the scatterers can be calculated by Fourier transforming chi(*k*). In the RDFs, the peak positions are correlated to average atomic distances, whereas the areas underneath the maxima are a measure of the average number of scattering atoms.[16] In Table 1 the number and radial distances of scatterers around a central O atom in crystalline ZnO are listed.

Figure 5 shows the RDFs for the films deposited under the highest water ambient conditions ($P_{H_2O} = 5 \times 10^{-4}$ mbar) for 30 and 50 Å thicknesses, respectively. The experimental curve for the 50 Å thick, self-textured film has been fitted using the automated code FEFF for ab initio curved wave calculations.[17] In the theoretical standard shells up to 4.6 Å radial distance from the central O atom were considered (see Table 1) and the fitting was performed in a Hanning window from 0 to 4 Å. Best fitting results were achieved using an amplitude factor $S_0^2 = 1.1$ for this data set with the Debye temperature for the O−Zn bond $\Theta_D = 800$ K. The fitting procedure found the radial distances of the first and second shell to be 1.88 ± 0.1 and

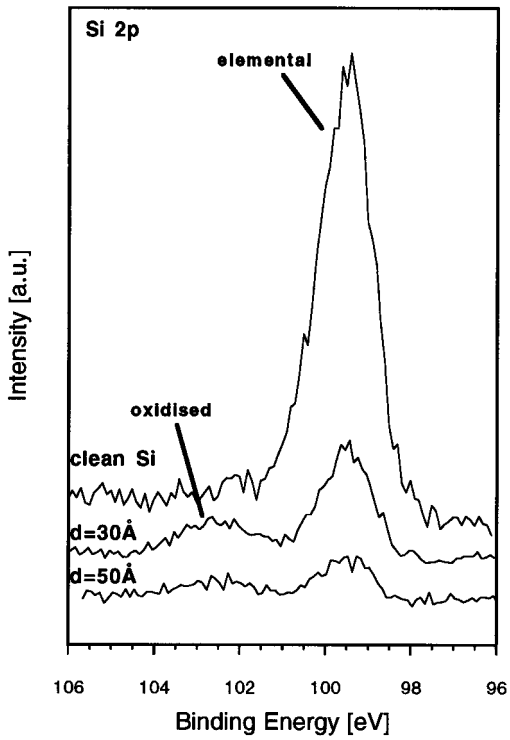


**Figure 4.** XPS spectra of the Si 2p photoelectron region as a function of deposited film thickness, *d*, with a water ambient of $5 \times 10^{-4}$ mbar at a surface temperature of 673 K.

**TABLE 1**

| shell no. | mean radial distance [Å] | atomic shell configuration [Å] |
|---|---|---|
| 1 | 1.98 | 1 Zn @ 1.97<br>3 Zn @ 1.98 |
| 2 | 3.23 | 6 O @ 3.21<br>1 Zn @ 3.24<br>6 O @ 3.25 |
| 3 | 3.80 | 6 Zn @ 3.80<br>3 Zn @ 3.8 |
| 4 | 4.58 | 6 O @ 4.57<br>6 Zn @ 4.59 |

3.21 ± 0.1 Å, respectively, which is in good agreement with the expected values (see Table 1). In the curve for the thinner film (30 Å), the second-shell features are somewhat more complicated but do not exhibit the pronounced second-shell peak associated with the 12 O and 1 Zn neighbors in crystalline ZnO. This different atomic environment in the interfacial region is in agreement with the above model, where the nonstoichiometric, mixed film composition in this thickness range inhibits the formation of a continuous ZnO matrix and thus a film self-texture. From the present results it is concluded that the thickness of this interfacial region under the conditions required for growth of self-textured ZnO films from the BZA precursor is approximately 30 Å.

**(2) Film Growth Kinetics.** It has been suggested that the water ambient aids in the formation of textured ZnO films by improving the volatility of organic byproducts.[7] The self-texture would then be promoted due to a significant reduction in trapped film contaminants. In Figure 6, C 1s NEXAFS spectra of films deposited under the various water pressures are shown (thickness approximately 50 Å). The main features can be assigned to CC$\pi$* (at ∼285 eV), CH$\pi$*/C═O$\pi$* (at ∼288 eV), and CCs* (at ∼293 eV) resonances.[18] For comparison a C 1s NEXAFS spectrum obtained from a ZnO film deposited with no water ambient (thickness 20 Å) is shown in the inset in Figure 6.[14] No significant changes are evident once a water ambient is

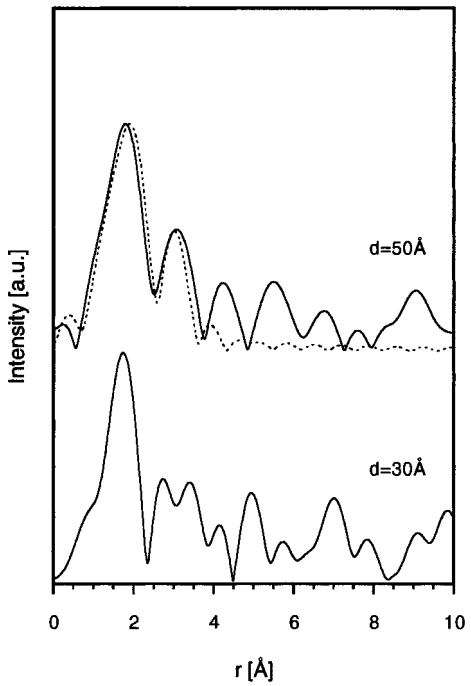


**Figure 5.** Fourier transforms of the O 1s SEXAFS region for deposition with a water ambient of $5 \times 10^{-4}$ mbar as a function film thickness, *d*, deposited at a surface temperature of 673 K. Dotted line is a curve fit of the experimental data using the FEFF code (see text for details).

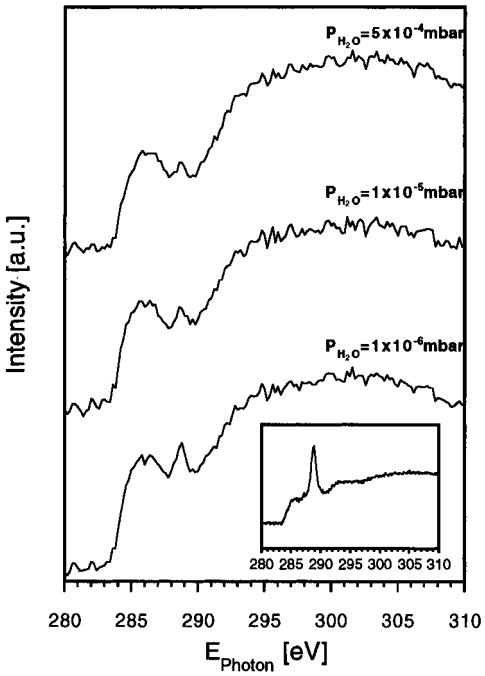


**Figure 6.** C 1s NEXAFS spectra as a function of water ambient used during the film deposition at a surface temperature of 673 K and film thicknesses approximately of 50 Å. The inlet shows the C 1s NEXAFS spectra for a 20 Å thick film deposited without a water ambient.[14]

present during the decomposition. This supports the previous report that the presence of a water ambient is very effective in the reduction of organic film contaminants. However the result that only small differences in the spectra for deposition in the different water ambient were found suggests that this mechanism alone cannot explain the high water pressure required to promote self-texture of the ZnO films.

Figure 7 shows the RDFs calculated from the O 1s SEXAFS data for the ZnO films deposited under the different water pressures used in this work. In all curves the strong first-shell

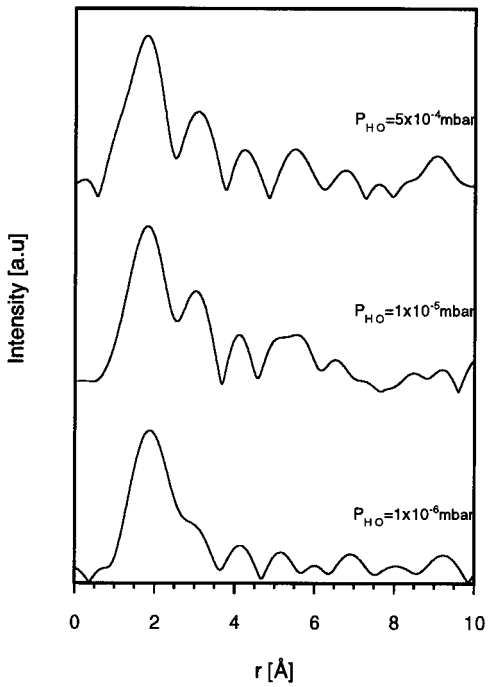


**Figure 7.** Fourier transforms of the O 1s SEXAFS regions for approximately 50 Å thick films as a function of water ambient used.

peak associated with the four nearest Zn neighbors is observed. With increasing water pressure, the intensity of the second-shell peak increases. This indicates that the atomic environment at the oxygen sites in the deposited film changes. If we consider the atomic configuration in crystalline ZnO (see Table 1), the reduced second-shell intensity might be related to oxygen vacancies in the deposited films. ZnO is known to form oxygen vacancies at the surface under high vacuum above room temperature. The formation of such defects is thermodynamically favorable due to the increase in the surface entropy, resulting in a lowering of the Gibbs free energy. Göpel et al.[19] reported that the surface concentration of oxygen vacancies can be reduced by a factor of 10 by increasing the oxygen partial pressure from $10^{-8}$ to $10^{-5}$ mbar at ZnO surface temperatures above 700 K due to dissociative surface reactions between chemisorbed oxygen and oxygen vacancies. The thermodynamical stability of nonstoichiometric $ZnO_{1-x}$ surface layers under high-vacuum and high-temperature conditions has to be considered in the CVD growth mechanism. Such layers can be formed when we consider more than one decomposition path for the BZA precursor. We will discuss the decomposition kinetics with two parallel reactions, the suggested pyrolysis of BZA to form stoichiometric ZnO,[20]

$$Zn_4O(CH_3COO)_6(g) \xrightarrow{k_1} 4ZnO(s) + 3CH_3OCH_3(g) + 3CO_2(g) \quad (1)$$

and the complete decarboxylation reaction of the BZA precursor,

$$Zn_4O(Ch_3COO)_6(g) \xrightarrow{k_2} Zn_4O(s) + 6CH_3COO(s^*) \quad (2)$$

resulting in oxygen vacancies in the deposited layers under high-vacuum, high-temperature conditions. The subsequent surface reactions in the presence of a water vapor could then be described by the following rate equations:

$$H_2O(g) \xrightarrow{k_{-3},\, s_{H_2O}} O(s) + 2H(s^*) \quad (3)$$

$$CH_3COO(s^*) + H(s^*) \xrightarrow{k_4} CH_3COOH(g) \quad (4)$$

$$Zn_4O(s) + 3O(s) \xrightarrow{k_5} 4ZnO(s) \quad (5)$$

where $s_{H_2O}$ is a sticking coefficient and $k_i$ are the rate constants of the form $\nu_n N^n e^{-E_A/kT}$, with $n$ describing the kinetic order, $n_n$ and $E_A$ the prefactor and activation energy, and $N$ the density of adsorption sites.[21]

In eqs 3−5 two roles of the water as (i) source of hydrogen for the hydrogenation of the precursor fragments to prevent secondary fragmentation and (ii) oxygen source required to form stoichiometric ZnO layers become evident. We suggest that the high water pressure required is related to the oxygen "incorporation" reaction in the above kinetic model (eq 4). From the reaction steps 3−5 a set of equations describing the formation of stoichiometric ZnO can be derived.

The change in the oxygen coverage is given by

$$\frac{\partial N_o}{\partial t} = \frac{s_{H_2O} P_{H_2O}}{\sqrt{2\pi m_{H_2O} kT}} - k_{-3}\theta_O\theta_H{}^2 - 3k_5\theta_o{}^3\theta_{Zn_4O} \quad (6)$$

and the amount of the $Zn_4O$ species varies according to

$$\frac{\partial N_{Zn_4O}}{\partial t} = -k_5\theta_o{}^3\theta_{Zn_4O} \quad (7)$$

Under steady-state conditions the oxygen coverage varies slowly with time so that its time derivative may be set to zero. If one further assumes that the quasi stationary hydrogen coverage $q_H \ll 1$ due to a high reaction rate in eq 4 at 673 K, the second-order term of $q_H$ in eq 6 may be neglected. Using eqs 6 and 7 the quasi stationary forward rate of eq 5 can then be written as

$$\frac{\partial N_{Zn_4O}}{\partial t} = -\frac{s_{H_2O} P_{H_2O}}{3\sqrt{2\pi mkT}} \quad (8)$$

The relation in eq 9 illustrates the dependence of the formation rate of stoichiometric ZnO on the water pressure used. Lattice stabilization due to improved stoichiometry in the deposited layers appears to be essential for a long-range self-texture within the deposited ZnO film in the absence of epitaxial promoted crystallization. A schematic of the proposed growth mechanism is given in Figure 8.

The influence of the vapor-phase composition during the ZnO crystal growth in conventional CVD using ZnO transport in hydrogen and reoxidation of the zinc vapor by oxygen has been studied intensively.[22,23] The presence of a water ambient during the growth was found to improve the perfection and physical properties of the ZnO crystals.[23] This was assigned to the reduced supersaturation of the reduction of ZnO:

$$ZnO(s) + 2H(s) \xleftrightarrow{k_{-9},\, k_9} Zn(g) + H_2O(g) \quad (9)$$

where the reaction direction is from right to left when it is performed in a high water concentration, i.e., under nonequilibrium conditions. Although the surface reactions in the growth of a ZnO film via thermal decomposition of an organometallic precursor differ significantly from reoxidation reactions in the $ZnO-H_2-H_2O-O_2$ system, it is interesting to note that the presence of a water pressure in the gas phase during the deposition will reduce the hydrogenation of ZnO. With this mechanism blocked, the hydrogenation of organic fragments becomes the predominant path for adsorbed H. This could explain the efficiency of the water ambient to reduce film contamination, where only insignificant changes occur between the highest and the lowest water pressures used (see Figure 6).

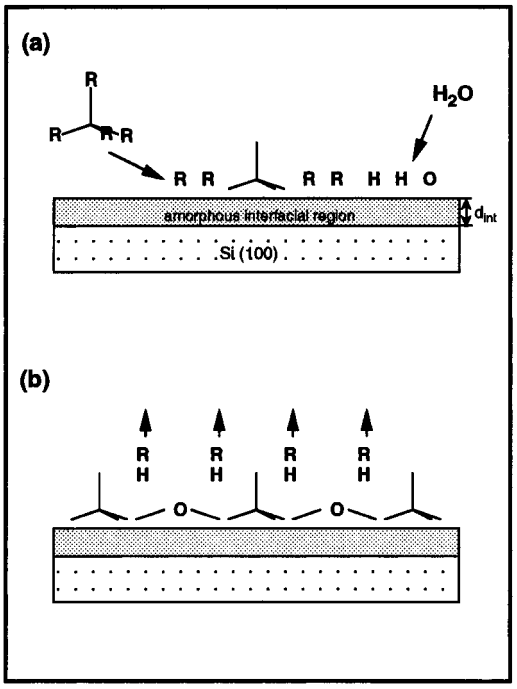


**Figure 8.** Schematic of the proposed kinetic model for the self-structuring of the ZnO tetrahedral fragments to form an oriented ZnO film at high-temperature, high water ambient conditions. The self-structuring occurs on top of an interfacial region formed during the oxidation of the substrate in the initial stages of film growth.

**(3) Nature of Interfacial Restrictions: Substrate Influence.** The results obtained for the Si(100)−ZnO model system might indicate some SS-CVD specific predispositions. The obtained self-texture of the films appears to be driven by an intrinsic crystallization of pure ZnO on top of an amorphous region comprising a mixture of ZnO and oxidized Si. Therefore both structural and "chemical" restrictions are apparent in the Si(100)−ZnO system. It is therefore interesting to study the growth on less reactive surfaces such as Pt and Au to investigate the influence of the chemical reactivity of the substrate material on the thickness of the interfacial "buffer" region, $d_{int}$ (see Figure 8). In addition to a low oxidation potential, the Au(111) surface exhibits a lattice mismatch to ZnO of only ∼10%. Such systems are currently used to study the transition between epitaxial promoted crystallization and the intrinsic self-texture of pure ZnO in this low-energy deposition technique.

From the present study, the results that the interfacial region formed on silicon (i.e. a high oxidation potential material) is only about 40 Å thick and a self-texture of the ZnO film is obtained for film thicknesses as low as 50 Å show the potential of the single-source CVD technique to grow oriented, polycrystalline films for applications in which the structural properties of the substrate−film interface strongly influence the device performance.

## Conclusions

The onset of self-texture in ZnO films grown by SS-CVD from a $Zn_4O(acetate)_6$ precursor on Si(100) in a high water ambient ($P_{H_2O} = 5 \times 10^{-4}$ mbar) at 673 K substrate temperature occurs for film thicknesses on the order of 50 Å. No self-texture was obtained for films deposited in lower water ambient for film thicknesses up to 80 Å. The self-texture appears to be promoted by lattice stabilization due to oxygen incorporation

into $ZnO_{1-x}$ surface layers to form more stoichiometric films, for which the (0001) plane is a singular plane. A parallel reaction decomposition mechanism for BZA on the heated Si(100) substrate is proposed, resulting in nonstoichiometric films when the deposition is performed under the high-vacuum (no water ambient), high-temperature conditions required in the process.

The interfacial restriction for CVD growth from an organometallic precursor on the Si(100) surface can be divided into two components: a chemical and a structural restriction. The chemical restriction is evident in the obtained oxidation of the Si substrate, which results in a mixed chemical composure of the interfacial region inhibiting growth of "pure" ZnO films from the immediate interface. To some extent that reduces the importance of the substrate structural restriction in such systems since the subsequent self-texture occurs on an amorphous buffer layer readily formed in the initial stages of film growth.

## References and Notes

(1) van de Pol, F. C. M. *Ceram. Bull.* **1990**, *69*, 1959.
(2) Fujimura, N.; Nishihara, T.; Goto, S.; Xu, J.; Ito, T. *J. Cryst. Growth* **1993**, *130*, 269.
(3) Hickernell, F. S. *IEEE Ultrason. Symp.* **1988**, 417.
(4) Persegol, D.; Pic, E.; Plantier, J. *J. Appl. Phys.* **1987**, *62*, 2563.
(5) Paradis, E. L.; Shuskus, A. J. *Thin Solid Films* **1976**, *38*, 131.
(6) Kushida, K.; Takeuchi, H. *J. Appl. Phys.* **1984**, *56*, 1133.
(7) Mar, G. L.; Timbrell, P. Y.; Lamb, R. N. *Chem. Mater.* **1995**, *7*, 1890.
(8) Ghijsen, J.; Tjeng, L. H.; van Elp, J.; Eskes, H.; Westerink, J.; Sawatzky G. A.; Czyzyk, M. T. *Phys. Rev. B* **1988**, *38*, 11322.
(9) Hartmann, A.; Russel, G. J. *Solid State Commun.* **1995**, *95*, 791.
(10) Holldack, C.; Grunze, M. *Anal. Chem. Acta* **1993**, *297*, 125.
(11) Koch, M. H.; Mar, G. L.; Hartmann; A. J.; Lamb, R. N. *Surf. Interface Anal.* **1996**, *24*, 675.
(12) Seah, M. P. *Practical Surface Analysis*, 2nd ed.; John Wiley & Sons Ltd.: Chichester, 1990; Vol. 1, Chapter 3.
(13) Mar, L. G.; Timbrell, P. Y.; Lamb, R. N. *Thin Solid Films* **1993**, *223*, 341.
(14) Koch, M. H.; Hartmann, A. J.; Lamb, R. N.; Neuber, M.; Walz, J.; Grunze, M. *Surf. Rev. Lett.* **1997**, *4*, 39.
(15) Katsikini, M.; Paloura, E. C.; Kalomiros, J.; Bressler, P.; Moustakas, T. *BESSY Jahresbericht 1995*; Gaupp, A., Ed.; BESSY: Berlin, 1996.
(16) For example: Henzler M.; Göpel; G. *Oberflächenphysik des Festkörpers;* Teubner: Stuttgart, 1991; Chapter 4.
(17) de Leon, J. M.; Rehr, J. J.; Zabinsky, S. I.; Albers, R. C. *Phys. Rev. B* **1991**, *44*, 4146.
(18) Stöhr, J. *NEXAFS Spectroscopy;* Springer: New York, 1992.
(19) Göpel, W. *J. Vacuum Sci. Technol.* **1978**, *15*, 1298.
(20) Hiltunen, L.; Leskela, M.; Makela, M.; Niinisto, L. *Acta Chem. Scand. A* **1987**, *41*, 548.
(21) Christmann, K. *Topics in Physical Chemistry, Vol. 1;* Steinkopff Verlag: Darmstadt, 1991.
(22) Pasko, P. G.; Kidyarov, B. I.; Avdienko, K. I. *J. Cryst. Growth* **1976**, *33*, 298.
(23) Au, C. T.; Roberts, M. W.; Zhu, A. R. *Surf. Sci.* **1982**, *115*, L117.